scientific reports

Check for updates

OPEN

Interfacial-active green surfactants from sugarcane bagasse and its biochar for enhanced oil recovery

Pegah Sarafzadeh[1], Feridun Esmaeilzadeh[2]✉, Kaveh Morshedi[2], Sedigheh Safarzadeh[3]✉ & Gholamreza Vakili-Nezhaad[4]

Sugarcane bagasse (SCB), a primary agricultural waste from sugar production, poses significant environmental challenges due to its accumulation. This study introduces the direct application of SCB and its biochar (SCB-B) as cost-effective and eco-friendly agents for Enhanced Oil Recovery (EOR). We systematically investigated their efficacy in reducing oil-water interfacial tension (IFT) and altering the wettability of carbonate rocks. Both materials significantly reduced IFT by up to 70% and shifted strongly oil-wet surfaces towards neutral-wet conditions by up to 47% at very low concentrations. A pivotal finding was the shift in governing mechanisms at the Critical Micelle Concentration (CMC), which increased from 16 ppm in distilled water to 70 ppm in saline environments. Interestingly, a reversal in the performance trends of SCB and SCB-B for wettability alteration was observed precisely at the CMC, attributed to a concentration-dependent agglomeration behavior of surface functional groups. While the ultimate IFT reduction is less pronounced than that of pure chemical surfactants or saponins, the key advantage of our approach lies in utilizing unprocessed agricultural waste directly, bypassing the need for costly and complex extraction procedures. This work establishes a dual-value proposition by offering a sustainable strategy for waste management and presenting an economically viable, green alternative to conventional chemical EOR agents.

Keywords Biochar, Sugarcane bagasse, Enhanced oil recovery, Green surfactants, IFT reduction, Wettability alteration

Sugarcane is one of the world's most productive crops, cultivated annually in countries like Brazil, India, China, and Thailand, contributing billions of dollars to the global economy[1]. Annually, over 1.9 billion tons of sugarcane are produced worldwide[2]. It plays a significant role in the global economy as a primary source of sugar and various valuable byproducts. However, following sugar extraction, approximately 30% of the sugarcane's weight remains as bagasse, a lignocellulosic waste material[3]. Chemically, bagasse comprises 40–50% cellulose, 20–30% hemicellulose, and 20–25% lignin, rendering it an ideal feedstock for biochar production[4]. The fibrous nature of sugarcane bagasse (SCB) is well-documented, consisting of cellulose surrounded by lignin and hemicellulose, with lignin being an aromatic biopolymer composed of diverse phenols and acids[5]. The chemical structures of these primary components are well-established in the literature[5,6].

Historically, this waste product was often burned or discarded in landfills, contributing significantly to air pollution and greenhouse gas emissions[7]. In contrast, bagasse is now recognized as a cost-effective and abundant resource for producing biochar—a polyaromatic carbon material generated through the thermochemical conversion of biomass under limited or no oxygen conditions, a process known as pyrolysis[8–12]. Biochar is widely regarded as an innovative solution for sustainable waste management, environmental remediation, and resource optimization[14–16]. It exhibits unique characteristics, including a high specific surface area, well-developed porosity, and active functional groups such as carboxyl (–COOH) and hydroxyl (–OH)[17]. The properties of biochar can vary significantly depending on the feedstock and production conditions, allowing it to be engineered for specific applications[18]. On a detailed level, many biochar properties stem from disordered valence sheets, resulting in unpaired electrons and unsaturated valences, typically providing more active sites compared to the original feedstock[19–21]. The presence of a significant number of non-local π electrons confers a

[1]Department of Engineering Sciences, Technical and Vocational University (TVU), Tehran, Iran. [2]Department of Chemical Engineering, School of Chemical and Petroleum Engineering, Shiraz University, Shiraz, Iran. [3]Department of Soil Science, School of Agriculture, Shiraz University, Shiraz, Iran. [4]Department of Petroleum and Chemical Engineering, Sultan Qaboos University, Muscat, Oman. ✉email: esmaeilzadeh95@gmail.com; rsafar2010@gmail.com

negative surface charge, enabling it to act as a Lewis base and adsorb Lewis acids via chemisorption or physical processes[21]. Furthermore, properties such as the ability to form hydrogen bonds, acid-base interactions, and the presence of surface-active functional groups containing nitrogen and oxygen enhance the performance of biochars in various fields, particularly as bio-adsorbents[21]. Numerous studies have examined the potential use of sugarcane bagasse-derived biochar (SCB-B) in various industries, highlighting its unique properties and high efficiency. For instance, recent publications reveal its honeycomb-like structure, which consists of a network of tiny, interconnected pores, increasing the surface area and enabling effective trapping of heavy metals[22]. Moreover, its thermal stability and graphene-like structures contribute to its durability and long-term effectiveness[23]. These properties make it highly effective for soil improvement, pollutant adsorption, and environmental remediation[16], as well as applications in water treatment and energy[13–27].

Despite the promising properties and diverse applications of SCB-derived biochar, a critical literature gap exists, as there is a severe lack of information regarding its potential use in oil and gas-related industries, particularly for Enhanced Oil Recovery (EOR). In recent decades, declining production from existing reservoirs, the high cost of discovering new ones, the increasing global demand for fuel resources, and the limitations of conventional EOR methods have prompted researchers to explore new avenues. Chemical enhanced oil recovery, which utilizes chemical surface-active agents, is one of the most important EOR methods. Although chemical surfactants demonstrate a strong ability to reduce interfacial tension, they face challenges such as environmental concerns, high adsorption losses, and high production costs[28]. This has driven the search for greener alternatives, such as biosurfactants from microorganisms[29–37] and natural surfactants extracted from plants[53–71]. Most published articles in the latter category aimed to extract saponin from different plant parts, which involves complex and costly processes[56,57,81]. However, no previous effort has been made to utilize plant-derived biochar or unprocessed plant waste in the manner proposed in this study for EOR applications. This work aims to fill this critical gap by exploring, for the first time, the potential of using raw sugarcane bagasse (SCB) and its biochar (SCB-B) as direct and green agents for enhancing oil recovery.

We hypothesize that the inherent amphiphilic nature, surface chemistry, and functional groups of SCB and SCB-B could enable them to act as effective green surfactants, facilitating adsorption at the oil-water interface and rock surface. This would reduce interfacial tension and alter wettability towards neutral conditions—two fundamental mechanisms in chemical EOR. Therefore, the primary objective of this study is to conduct a fundamental laboratory investigation into the EOR potential of SCB and SCB-B. The specific aims are to: (1) characterize the physicochemical and structural properties of SCB and SCB-B; (2) quantify their ability to reduce oil-water IFT and determine their Critical Micelle Concentration (CMC) under both non-saline and saline conditions; (3) evaluate their efficacy in altering the wettability of carbonate rocks from both water-wet and oil-wet states; and (4) elucidate the underlying mechanisms governing their performance, with particular focus on the effects of salinity and concentration. In this regard, sugarcane bagasse was subjected to pyrolysis after preparation. The resulting biochar, along with the raw bagasse, underwent initial tests to determine their structures and chemical characteristics. Subsequently, the two main parameters governing chemical EOR, interfacial tension (IFT) and wettability, were evaluated in the presence of SCB and SCB-B at different concentrations under non-saline conditions. In the final part of the research, the effect of salinity was investigated by adding different concentrations of NaCl and $MgCl_2$, representing mono- and divalent salts. Optimal conditions were identified for both non-saline and saline environments. Finally, the underlying mechanisms were interpreted in detail.

Materials and methods

Materials

Preparation of sugarcane bagasse and its biochar

In this research, sugarcane bagasse (SCB) was first washed several times with deionized water to remove impurities, then dried at 60 °C for 48 h and subsequently ground using a mechanical grinder. The crushed samples were then pyrolyzed in an electric furnace under oxygen-limited conditions for 3 h at 350 °C. The produced biochar (SCB-B) was passed through a 2 mm sieve and stored in plastic containers for testing. The reproducibility of the synthesis process was confirmed by producing two separate batches.

Elemental analysis (carbon, hydrogen, and nitrogen) of the biomass and biochar samples was determined using a CHNS analyzer (vario MACRO CHNS). Additionally, the specific surface area of the materials was investigated using the Brunauer-Emmett-Teller (BET) method (Belsorp mini II, Microtrac Bel Corp, Japan). Finally, additional characteristics of both SCB and SCB-B were assessed by Fourier Transform Infrared Spectroscopy (FTIR; TENSOR II from Bruker). The results are presented in Table 1; Fig. 1, respectively.

The data presented in Table 1 show that the percentage of carbon in the resulting biochar increases. In contrast, the percentage of oxygen decreases, resulting in an O/C ratio in the biochar that is somewhat lower than that of the initial sugarcane bagasse. Published articles indicate that this ratio is directly related to the hydrophilicity of the sample under study, which suggests the amount of polar functional groups present in the sample; however, violations in this regard have also been reported in the literature[72,73]. In addition, the H/C ratio indicates the degree of carbonization and aromaticity in the samples studied[67,68]. Some articles point out that an H/C ratio above 0.7 can indicate the presence of aromatic substances with a structure similar to that of lignin and cellulose[53].

Additionally, Fig. 1 displays the FTIR spectra of raw sugarcane bagasse (SCB) and its pyrolyzed derivative, sugarcane bagasse biochar (SCB-B), highlighting key transformations in surface chemistry that directly influence their hydrophilic/hydrophobic behavior, particularly under conditions relevant to oil recovery.

In the raw SCB spectrum, the presence of strong absorption bands around 2930 cm^{-1} and 2850 cm^{-1}, corresponding to the C–H stretching vibrations of aliphatic $–CH_2$ and $–CH_2$ groups, indicates a high content of non-polar, hydrophobic moieties typical of lignocellulosic biomass. These aliphatic chains, derived from hemicellulose, cellulose, and lignin, are well-known for imparting hydrophobic character to biomass surfaces.

Properties	SCB	SCB-B
C (%)	39.5	51.42
H (%)	5.4	1.6
N (%)	0.57	1.1
EC (dsm^{-1})*	1.28	2.9
O (%)	54.62	49.1
K (%)	1.85	0.63
C/N	82.15	62.11
O/C	1.21	0.97
H/C	1.72	0.81
S_{BET} ($m^2\ g^{-1}$)	4.8	85.6

Table 1. Physicochemical and elemental characteristics of sugarcane bagasse (SCB) and sugarcane bagasse biochar (SCB-B). *1:10 sample/deionized water ratio.

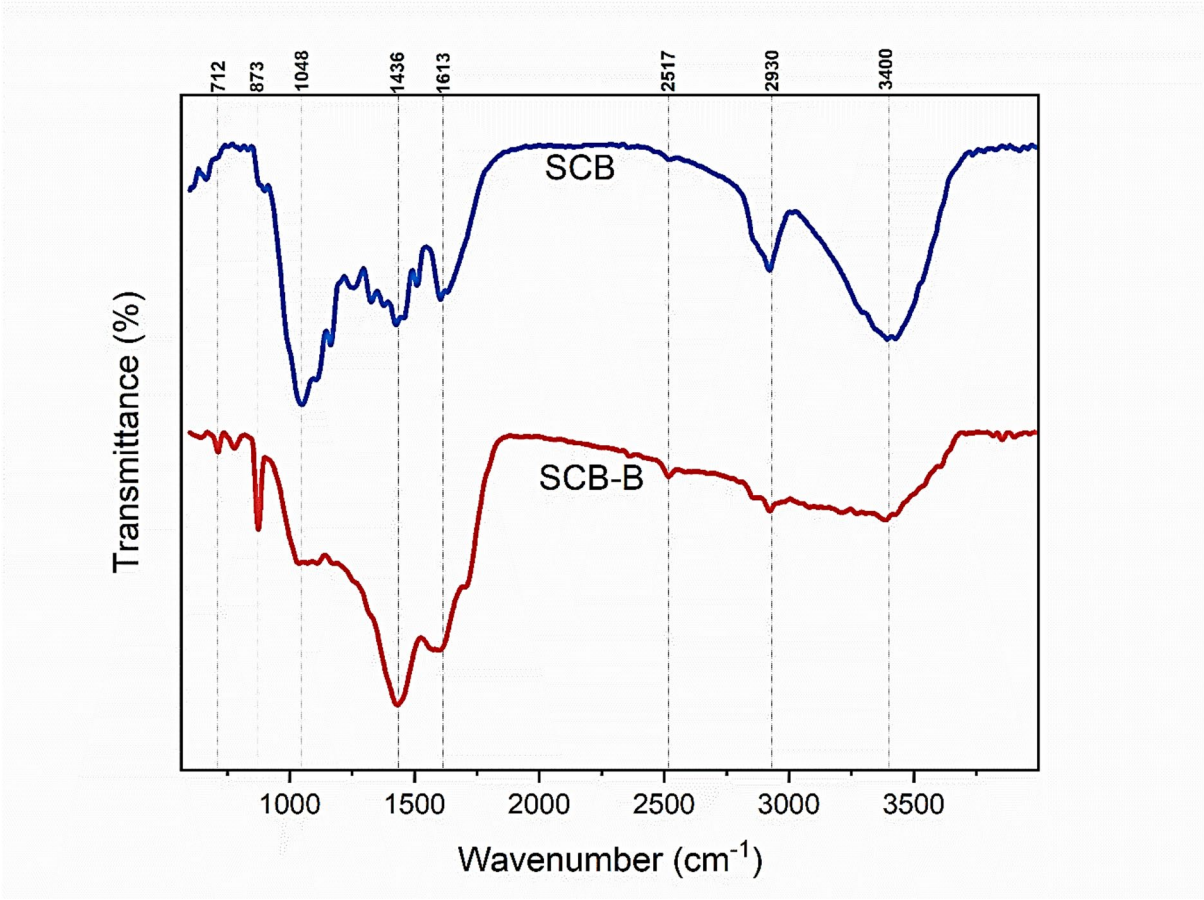

Fig. 1. Fourier transform infrared spectroscopy (FTIR) of SCB and SCB-B.

Upon pyrolysis, these aliphatic bands are strongly attenuated or even disappear, confirming the thermal degradation and volatilization of hydrophobic aliphatic compounds. Simultaneously, although some hydroxyl (O–H, ~ 3400 cm^{-1}) and ether (C–O, ~ 1048 cm^{-1}) groups are also lost, the spectrum of SCB-B shows a sharper and more prominent peak at 1436 cm^{-1}, assigned to carboxylate (COO^-) or oxygenated aromatic groups. This suggests that during pyrolysis, part of the oxygen-containing functionalities is not eliminated but are transformed and stabilized in more thermally resistant forms.

Contrary to the common assumption that biochars are always more hydrophobic due to increased aromaticity, the removal of hydrophobic aliphatic chains and the retention or restructuring of polar, oxygenated groups on the surface of SCB-B can increase its net hydrophilicity, especially in aqueous or saline environments.

In summary, the hydrophobicity of raw SCB is primarily driven by its abundant aliphatic content. At the same time, the pyrolysis process disrupts this structure, reducing hydrophobic groups and exposing or concentrating certain hydrophilic functionalities.

Properties of crude oil

Ilam crude oil, Bangestan formation, obtained from Ahwaz, Iran, was used for all tests.To provide a comprehensive characterization of the reservoir fluid, key physicochemical properties of the crude oil used in this study are presented in Table 2. All experiments were conducted under ambient laboratory conditions (25 °C and atmospheric pressure) as a fundamental proof-of-concept investigation.

Methods

IFT measurements

In the first stage of this study, dynamic IFT measurements and CMC calculations were performed using different SCB and SCB-B concentrations, ranging from 0 to 200 ppm, specifically at 5, 10, 16, 30, 50, 70, 80, and 100 ppm. All IFT measurements were conducted at ambient conditions (25 °C) using the pendant drop method with a DSA 100 instrument (KRŰSS GmbH, Germany). Each measurement was performed in triplicate, and the average values are reported. The CMC values were evaluated based on the prepared dynamic IFT curves for each compound and used for subsequent experiments under non-saline conditions.

Additionally, to assess the effect of salinity (from mono- and divalent salts) on the results, IFT values were re-measured at different concentrations of NaCl and $MgCl_2$ (0, 1000, 2000, 5000, and 50,000 ppm), representing various salinity conditions prevalent in oil reservoirs. The new CMC was determined based on the obtained dynamic IFT curves in the presence of different salinities and used for the next part of the experiments. In this stage, the concentration of both SCB and SCB-B was varied simultaneously with the salt concentration across the range of 0, 5, 15, 30, 70, 80, 100, and 200 ppm. NaCl and $MgCl_2$ were procured from Merck KGaA, Germany.

Contact angle measurements

To evaluate the effect of SCB and SCB-B on the wettability of the oil/water/rock system, contact angle measurements were performed on both clean (water-wet) carbonate rock slab surfaces and oil-aged carbonate rocks (considered oil-wet surfaces). The preparation steps for both rock surface types were as follows:

- Water-wet surfaces: First, the carbonate rock surfaces were washed twice with distilled water and then completely dried at a constant temperature of 80 °C. The cleaned surfaces were then immersed in a solution containing the sample under investigation for 15 days[65]. Finally, their contact angle was determined using a DSA 100 instrument (KRŰSS GmbH, Germany).
- Oil-wet surfaces: First, the surfaces were placed in an ultrasonic bath for 2 h at 125 watts to remove cutting debris and other foreign materials from the surface and internal pores. Afterward, they were completely dried at a constant temperature of 80 °C. The cores were then placed in sealed vessels containing crude oil for 22 days to render the rock surfaces oil-wet[65,75–78]. This 22-day aging period was selected based on established protocols in the literature to ensure consistent and stable oil-wet conditions. Finally, the cores were cleaned and used for contact angle measurements following the same procedure as for the water-wet surfaces.

All contact angle measurements were performed in triplicate under ambient conditions. The standard deviation for these measurements was less than 3°, indicating good reproducibility.

Colloidal characterization: particle size and surface charge analysis

Particle size (hydrodynamic diameter) and surface charge (zeta potential) analyses were conducted to investigate the aggregation behavior and interfacial properties of SCB and SCB-B dispersions. The measurements were performed using a Dynamic Light Scattering instrument (Model: SZ-100, Horiba, Japan) equipped with a solid-state laser operating at a wavelength of 532 nm and a power of 10 mW. Measurements were performed at a scattering angle of 13° for optimal determination of both particle size and zeta potential. The instrument

Property	Value	Method/standard
API gravity	23.4	ASTM D70
Asphaltene content (%)	5.7	IP 143
Resin content (%)	18.0	SARA analysis
Saturates (%)	45.1	SARA analysis
Aromatics (%)	31.2	SARA analysis
Viscosity @ 25 °C (cP)	42.5	ASTM D445
Density @ 25 °C (g/cm^3)	0.912	ASTM D4052
Total Acid Number (TAN, mg KOH/g)	0.35	ASTM D664
Baseline IFT vs. water (mN/m)	30.1	Pendant drop

Table 2. Physicochemical properties of the Ilam crude oil (Ilam field) used in this study.

measures the electrophoretic mobility of particles, which is converted to zeta potential using the Smoluchowski equation.

Sample suspensions were prepared at specific concentrations (10 ppm and 200 ppm) in deionized water. Each suspension was homogenized using a probe sonicator operating at 30% amplitude for 5 min immediately prior to analysis to ensure dispersion. All measurements were performed at a constant temperature of 25 °C.

To ensure statistical reliability and reproducibility, each particle size (DLS) measurement was repeated nine times ($n = 9$), and each zeta potential measurement was repeated four times ($n = 4$) for every sample condition. The mean values, along with the standard deviation, are reported. These data provide direct evidence for the concentration-dependent aggregation and conformational changes discussed in "Investigating the reversal in colloidal behavior ofSCB and SCB-B across the CMC".

Results and discussion

Dynamic IFT measurements and CMC calculations

Dynamic IFT curves obtained from IFT measurements at different concentrations of SCB and SCB-B are depicted in Fig. 2.

As shown in Fig. 2, the interfacial tension decreases from an initial value of approximately 30 mN/m to final values of 12.98 mN/m and 15.45 mN/m for SCB and SCB-B, respectively. This reduction demonstrates that both SCB and SCB-B can be classified as new natural (green) surfactants. While their performance is within the acceptable range observed for other plant-based and microbial-based surfactants[1–3,34,35,37,54,67,81–87], greater IFT reductions have been reported in the literature using purely extracted saponin from plants or chemical surfactants[28,81].

As noted earlier, although chemical surfactants can reduce IFT to much lower values (even below 1 mN/m), limitations such as environmental concerns, high costs, and significant adsorption drive the search for new candidates. The performance of SCB and SCB-B is comparable to other natural surfactants; for instance, a crude biosurfactant from *Bacillus Stearothermophilus* SUCPM#14 reduced IFT from 30 mN/m to 14.5 mN/m[3], whereas *Enterobacter Cloacae* lowered it to about 1.5 mN/m[1].

Similarly, studies on plant-derived surfactants report comparable performance. Chhetri et al. (2009) observed a reduction in IFT from 19 mN/m to 2.5 mN/m using a natural surfactant extracted from soapnut tree leaves[56]. Ahmadi et al. (2012) reported a 69% IFT reduction using a surfactant from *Glycyrrhiza Glabra*[57], and Deymeh et al. (2012) demonstrated IFT reduction from 32 mN/m to 9 mN/m above CMC using a natural cationic surfactant[53]. The key advantage of using raw SCB and SCB-B lies in their origin as low-cost agricultural wastes requiring minimal processing, offering a significant economic and environmental benefit despite a potentially lower performance compared to purified agents. In other words, the innovation of this study is that using agricultural waste directly, without extensive processing, yields a satisfactory IFT reduction. It is important to note that IFT reduction is not the sole factor in enhancing oil recovery; parameters like wettability alteration can have an even more substantial impact[3].

Notably, raw SCB achieves a greater IFT reduction than SCB-derived biochar. This can be attributed to the reduction of aliphatic functional groups on the biochar surface during pyrolysis, as confirmed by FTIR analysis. Since the hydrophobicity of biochars is directly proportional to their aliphatic group content[85–87], SCB-B possesses fewer of these groups than raw bagasse, making it more hydrophilic. Consequently, the more hydrophobic raw bagasse has a higher tendency to migrate from the aqueous phase to the oil/water interface, leading to a greater IFT reduction.

Furthermore, the IFT stabilizes at concentrations above 16 ppm, indicating the Critical Micelle Concentration (CMC) under non-saline conditions. This low CMC value is an advantage for SCB and SCB-B, as other plant-derived surfactants often require significantly higher concentrations to reach their CMC[65–81].

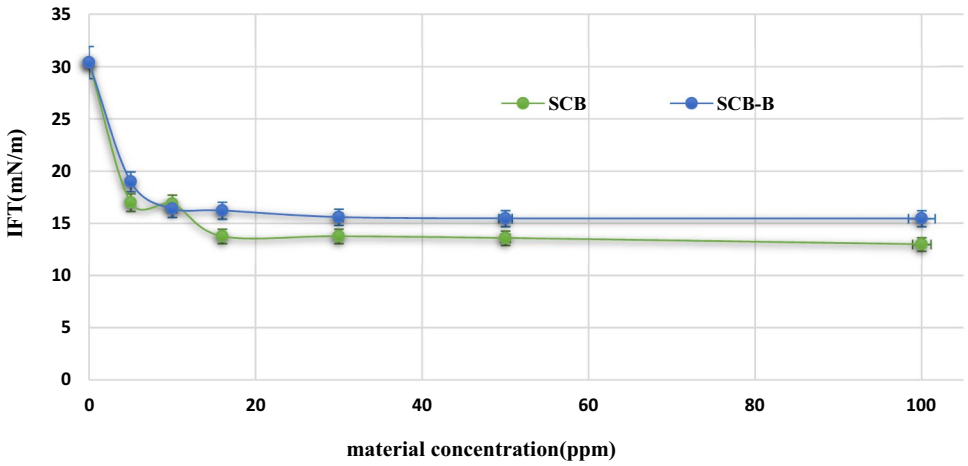

Fig. 2. Dynamic IFT measurements of SCB and SCB-B at concentrations ranging from 0 to 200 ppm in deionized water at 25 °C. Typical experimental variability ranges from ± 0.2 to 0.3 mN/m across measured IFT values.

Wettability alteration of water-wet and oil-wet carbonated surfaces

Figures 3 and 4 show wettability alteration caused by SCB and SCB-B for water-wet and oil-wet rock surfaces, respectively. All contact angle values are the average of at least three measurements on different spots of the rock samples.

The results of these two figures show significant alterations in wettability induced by both SCB and SCB-B for both water-wet and oil-wet rock surfaces. This means that, in both types of surfaces, by using a very low amount of materials prepared at negligible or zero cost, the wettability of both oil-wet and water-wet surfaces approaches neutrally wet conditions.

A key point to consider for a better interpretation of the graphs is that, for water-wet surfaces, the goal is to increase the wettability of the surface to naturally wet conditions; whereas, for oil-wet types, it should be decreased. Therefore, in Fig. 3, the higher value in the graph represents better wettability, while in Fig. 5, the lower value observed in the chart shows higher wettability alteration.

Therefore, it can be deduced that at low concentrations (below the CMC), bagasse biochar generally performs better for water-wet surfaces, while raw sugarcane bagasse yields better results for oil-wet types. However, the difference in the obtained results is not considerable. However, at high concentrations (concentrations higher than CMC), the conclusion is reversed. This means that, at higher concentrations, raw sugarcane bagasse (SCB) performs better on water-wet surfaces, and its biochar generally yields better results on oil-wet surfaces. In other words, although the amount of differences in the results obtained, in some cases, is minimal, surprisingly, results show that for both water-wet and oil-wet surfaces, the trend observed in the results changes at the CMC, which declares a switch in dominant governing mechanisms.

The reason can be found in the fact that, at concentrations lower than CMC, SCB-B with a hydrophilic surface has a better performance in changing the wettability of the water-wet surfaces, and in contrast, SCB with

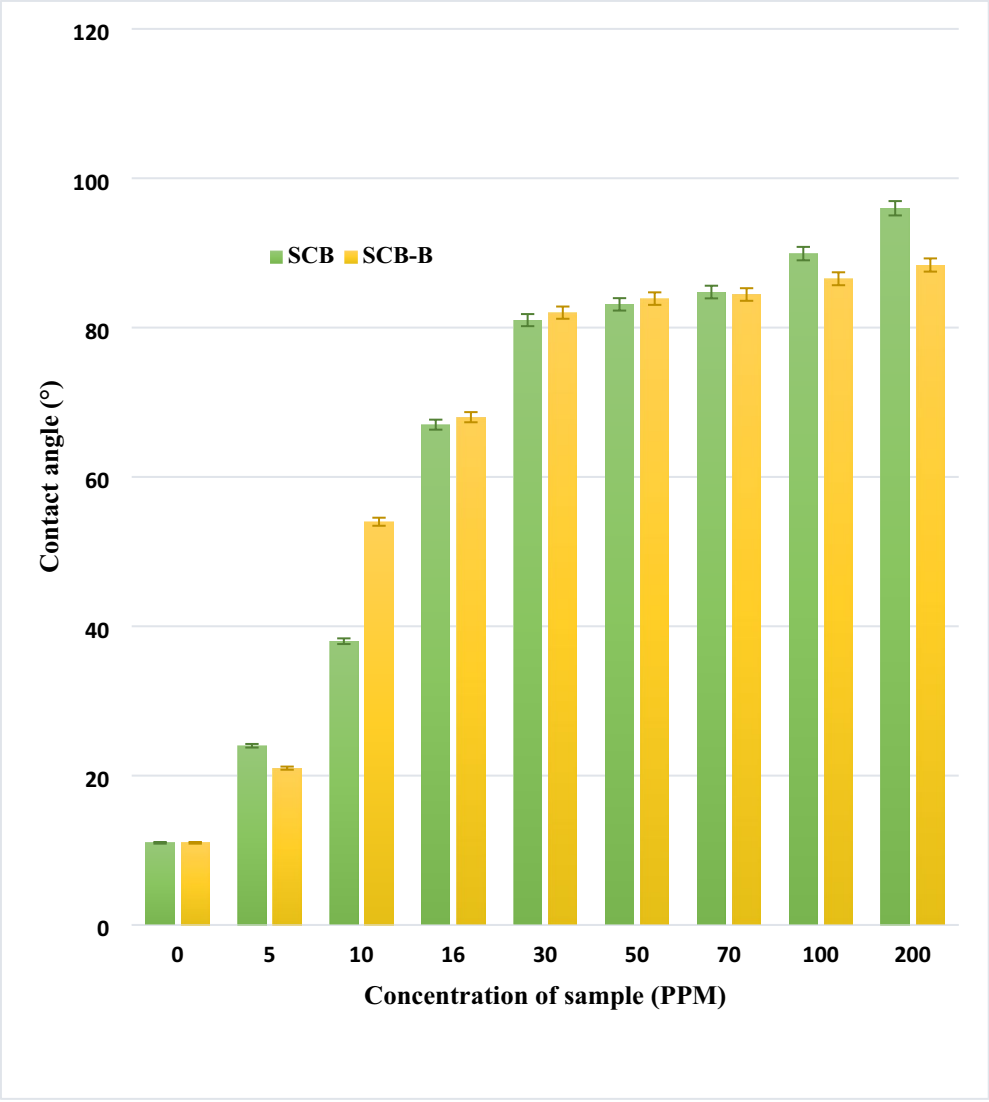

Fig. 3. Contact angle measurements on water-wet surfaces at different concentrations of raw bagasse and bagasse biochar.

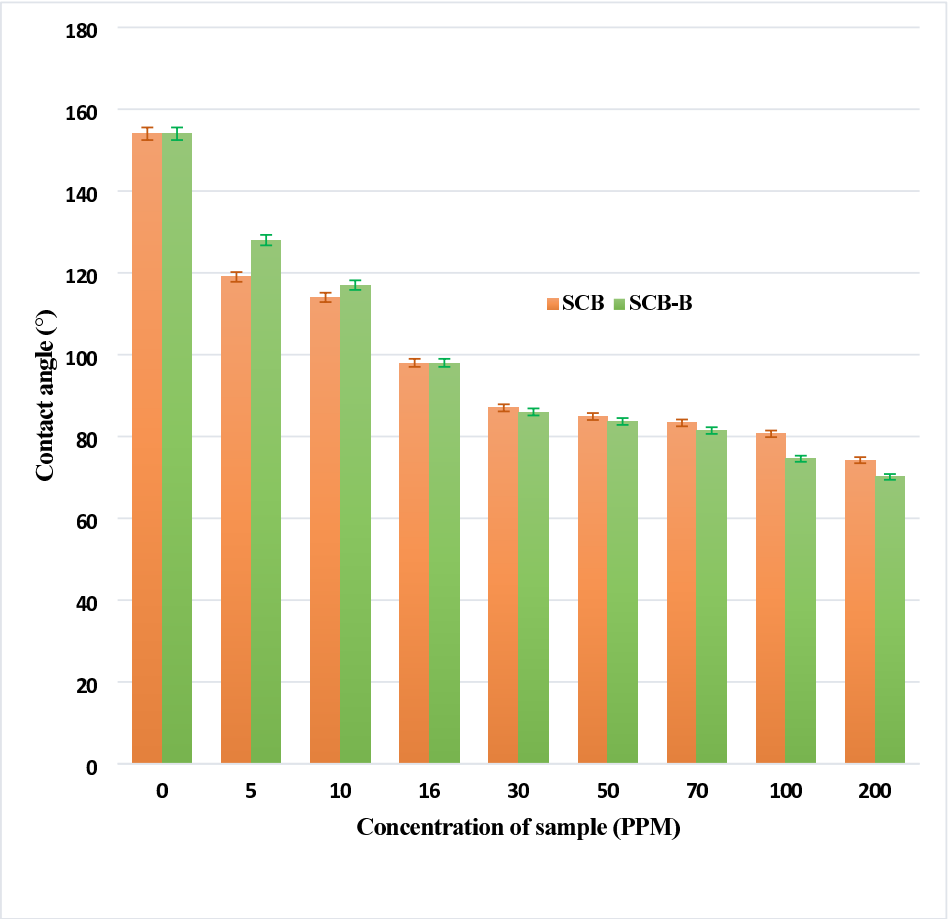

Fig. 4. Contact angle measurements on oil-wet surfaces at different concentrations of raw bagasse and bagasse biochar. Error bars represent the typical experimental variability, which ranges from ± 1° to 3° across the measured contact angle values.

a higher hydrophobicity has a better performance in changing the wettability of the oil-wet types. However, the opposite trend observed at concentrations higher than CMC can be attributed to the agglomeration of aliphatic groups on the surface of adjacent biochar molecules due to the increase in the concentration of biochar. In more detail, as stated, the aliphatic groups on the surface of biochar are the primary factor in the hydrophobicity of these molecules. As the SCB-B concentration increases in an aqueous medium, the aliphatic groups on the surface of adjacent molecules can interact with each other, accumulating, clumping, and eventually separating from the biochar's surface, which reduces the hydrophobicity. This phenomenon continues to the point where the hydrophobicity of the biochar surface decreases to the point where it is less than that of raw bagasse. In this case, bagasse will be a more hydrophobic material, and the bagasse biochar will be a more hydrophilic one. This phenomenon results in a shift in the role of these two materials at high concentrations. A similar phenomenon was observed in several articles regarding protein folding in aqueous media, resulting from agglomeration of aliphatic side chains[87,88].

Investigating the reversal in colloidal behavior of SCB and SCB-B across the CMC

To directly validate the hypothesis of aliphatic group agglomeration and to provide a unified colloidal-scale explanation for the behavioral shifts in both SCB and SCB-B, comprehensive particle size (Dynamic Light Scattering-DLS) and zeta potential analyses were conducted across the critical concentration range. The results are presented in Table 3.

The data in Table 3 reveal a fundamental divergence in the colloidal response of SCB and SCB-B to increasing concentration. For SCB, increasing the concentration from 10 ppm to 200 ppm resulted in a significant increase in surface charge negativity (from − 23.33 mV to − 33.60 mV) concurrent with a decrease in hydrodynamic diameter (from 274.3 nm to 232.1 nm). This phenomenon is characteristic of molecular uncoiling and surface reorganization[89,90]. At low concentrations, the flexible lignocellulosic polymers of SCB can adopt a coiled conformation in the aqueous phase, trapping polar groups and presenting a larger hydrodynamic volume with a less negative effective surface charge. Upon exceeding the CMC, the thermodynamic drive for interface stabilization prompts the molecules to unfold, exposing a greater number of ionizable, negatively charged

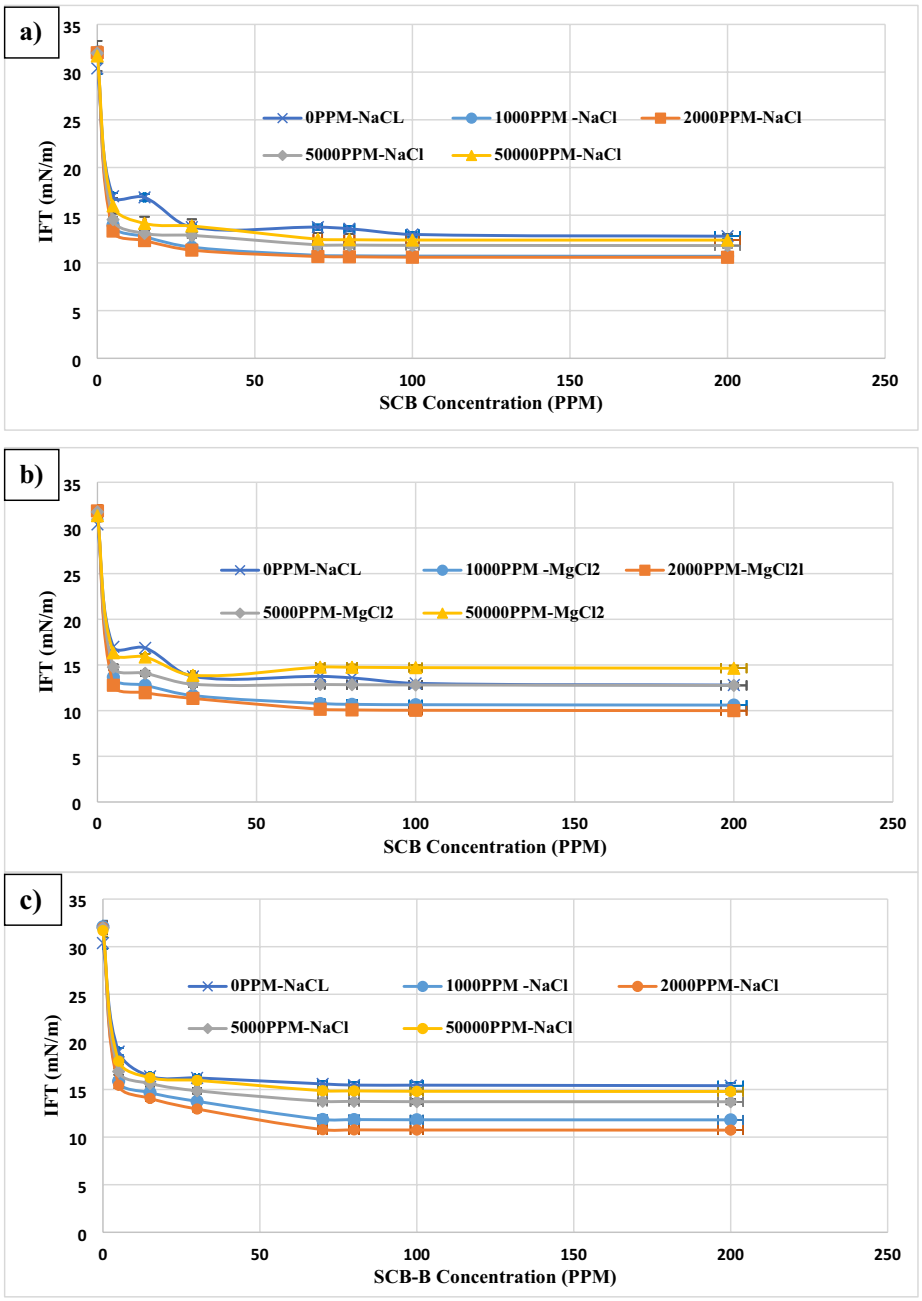

Fig. 5. Effect of salinity on IFT reduction by SCB and SCB-B: (**a**) SCB + NaCl, (**b**) SCB + $MgCl_2$, (**c**) SCB-B + NaCl, (**d**) SCB-B + $MgCl_2$. Typical experimental variability ranges from ± 0.2 to 0.3 mN/m across measured IFT values.

functional groups to the aqueous environment, thereby increasing the zeta potential and leading to a more compact hydrodynamic structure[71].

In stark contrast, SCB-B exhibited the opposite trend. Its hydrodynamic diameter increased markedly from 268.9 nm to 474.0 nm with increasing concentration, while its zeta potential showed a definitive decrease in negativity (from − 31.30 mV to − 29.4 mV). This behavior is indicative of a colloidal agglomeration mechanism driven by hydrophobic interactions. The pyrolysis process creates a rigid, aromatic carbon structure in SCB-B, as evidenced by the significant increase in surface area (S_{BET} from 4.8 to 85.6 m^2/g, Table 1) and the sharp decrease in the H/C ratio (from 1.72 to 0.81, Table 1), confirming advanced carbonization and loss of aliphatic moieties[72,91]. The FTIR analysis (Fig. 1) further confirms the attenuation of aliphatic C–H stretches (~ 2930 cm^{-1}) in SCB-B compared to SCB. However, the residual aliphatic groups on the rigid biochar surface become dominant at high concentrations (> CMC). The proximity of adjacent SCB-B particles facilitates hydrophobic interactions between these residual aliphatic chains, leading to agglomeration and an increase in apparent

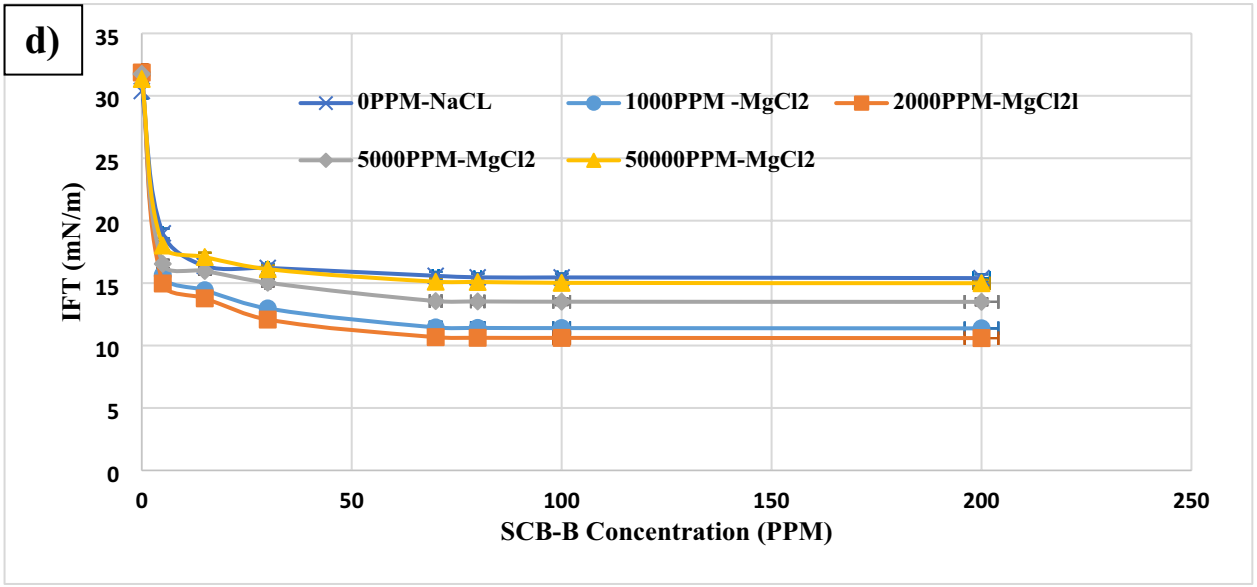

Fig. 5. (continued)

Sample	Concentration (ppm)	Hydrodynamic diameter (nm)	Zeta potential (mV)
SCB	10	274.3 ± 15.2	− 23.33 ± 1.5
	200	232.1 ± 12.8	− 33.60 ± 2.1
SCB-B	10	268.9 ± 14.6	− 31.30 ± 1.8
	200	474.0 ± 24.3	− 29.4 ± 0.6

Table 3. Hydrodynamic diameter and zeta potential of SCB and SCB-B dispersions below and above CMC under salt-free conditions. DLS measurements were repeated nine times ($n = 9$) and zeta potential analyses were conducted with four replicates ($n = 4$) for each sample. Values represent mean ± standard deviation.

particle size[85,86]. This agglomeration partially shields the underlying negatively charged aromatic surfaces, resulting in the observed slight reduction in zeta potential magnitude.

This mechanistic divergence—uncoiling for flexible SCB chains versus agglomeration for rigid SCB-B particles—provides a robust explanation for the reversal of their performance in altering the wettability of oil-wet and water-wet surfaces above the CMC, as detailed in the previous section. The unfolding of SCB exposes more hydrophilic groups, enhancing its interaction with water-wet surfaces. Conversely, the agglomeration of SCB-B reduces its surface hydrophobicity, favoring its interaction with and alteration of oil-wet surfaces. These insights bridge the gap between molecular-scale surface chemistry and macroscopic interfacial phenomena.

Results of IFT reduction in the presence of salinity

In this stage, NaCl and $MgCl_2$ with concentrations of 0, 1000, 2000, 5000, and 50,000 ppm were utilized to investigate IFT reduction with different concentrations of SCB and SCB-B in the range of 0, 15, 30, 50, 70, 80, 100, and 200 ppm in the presence of salinity (see Fig. 5 parts a to d). Data points in the figure represent the mean values from triplicate experiments.

Based on all parts of this figure, the optimum salinity of about 2000 ppm for both types of materials in the presence of both NaCl and $MgCl_2$ can be observed. In other words, SCB and SCB-B in the presence of NaCl and $MgCl_2$ show a decreasing-increasing trend in IFT. This means that by increasing the salt concentration, IFT reduces from its initial value, equal to the no-salinity condition, up to 2000 ppm salinity, and then it starts to increase. Meanwhile, in high salinity conditions (50,000 ppm), IFT approaches the value of the no-salinity condition. This trend has been observed in several articles[4,7,71,74]. For example, Lashkarboluki and his coworkers investigated the IFT reduction of an acidic oil containing asphaltene by several salts, such as Na_2SO_4 and $MgSO_4$, at different concentrations. Their results show an optimum salinity of 15,000 ppm for these salts in obtaining the minimum IFT reduction[74]. Additionally, Razzaghi-Koolaee et al. in 2022 investigated the effect of other types of salinity on a plant-derived surfactant (ARPE), and the same trend was observed in the IFT reduction curves[65].

This observed trend in IFT reduction can be explained by several mechanisms. At lower salinities, the salting-in effect can be an important mechanism. In more detail, the salting-in effect, which occurs due to the presence of special ions, such as Na^+ and Mg^{2+}, resulting from the dissolution of NaCl and $MgCl_2$ in water, and subsequent saponification, enhances the solvation of polar compounds like SCB and SCB-B[65]. Also, it is proven that the presence of salinity improves the SCB and SCB-B molecular mobility (acting as new surfactants) and

subsequently promotes migration of these molecules from the bulk into the oil/water interface[53,74]. Moreover, the presence of salt in the aqueous bulk can cause compression of the double layer, resulting in the molecules of SCB and SCB-B being placed at a much closer distance to each other at the oil/water interface, which leads to a reduction in IFT[53].

However, at higher salt concentrations, the salting-out effect dominates any fluid/fluid interaction, i.e., SCB and SCB-B, which are polar compounds, tend to transfer toward the oil phase; therefore, their solubility in the water phase is diminished[65]. Additionally, salinity disrupts the hydrated shield surrounding the ions present on the surface of SCB and SCB-B, which alters the balance at the water/oil interface, leading to an increase in the obtained IFT[53].

Another point that can be observed from these figures is that, in all cases, the IFT does not change considerably at concentrations higher than approximately 70 ppm. Therefore, this concentration can be considered the evaluated CMC in the presence of salinity for both SCB and SCB-B. However, as shown in the previous section, in no-salinity conditions, the calculated CMC is equal to 16 ppm. This indicates that the addition of salinity, even at low concentrations, increases the CMC value to approximately 70 ppm, demonstrating a dual effect of salinity on the reduction of interfacial tension for both SCB and SCB-B. In other words, by finding the optimal salinity, the interfacial tension can decrease, but the CMC increases.

In the next stage, to investigate the exact effect of salt type on the IFT reduction of both examined compounds, IFT results at optimum salinity (2000 ppm) in the presence of both SCB and SCB-B with NaCl and $MgCl_2$ are refigured and shown in Fig. 6.

As shown in this figure, at low concentrations of SCB and SCB-B (below the CMC), the difference in the calculated interfacial tension is more pronounced. In this condition, SCB in the presence of $MgCl_2$ and SCB-B in the presence of NaCl give the best and worst IFT reduction, respectively. However, with increasing concentrations of the materials (above the CMC value), the difference in ultimate IFT results decreases. Notably, at 200 ppm of the materials, raw bagasse in the presence of $MgCl_2$ leads to the highest IFT reduction, with a very small difference from the others, while the remaining conditions yield almost the same result.

In several articles, the greater ability of divalent cations (such as Mg^{2+}) compared to monovalent cations (like Na^+) in helping to further reduce interfacial tension by surfactants or other similar materials has been observed[74–88,92]. For example, Lashkarboluki et al. investigated the effect of different salts on the interfacial tension of acid oil containing asphaltene and concluded that divalent ions have a greater ability to reduce interfacial tension than monovalent ones.

As concluded from the IFT reduction of SCB and SCB-B in salt-free conditions, SCB exhibits a greater ability to reduce interfacial tension due to its inherently higher content of surface functional groups, particularly hydroxyl (OH^-) groups, as indicated by FTIR analysis (Fig. 2). These negatively charged hydroxyl groups interact with the positive cations (Na^+ and Mg^{2+}) from dissolved salts, thereby reducing the overall negative charge on the SCB surface. Additionally, since the boundary layer of oil and water has a negative charge, SCB molecules with a lower negative charge on their surface can more effectively approach the interface and reduce the IFT. However, divalent Mg^{2+} has a greater ability to change the surface charge of sugarcane bagasse because each Mg^{2+} ion simultaneously enters into ionic interaction with two adjacent hydroxyl groups on the surface of SCB, while each Na^+ interacts with one hydroxyl group (OH^-). The same phenomenon also occurs in the case of bagasse

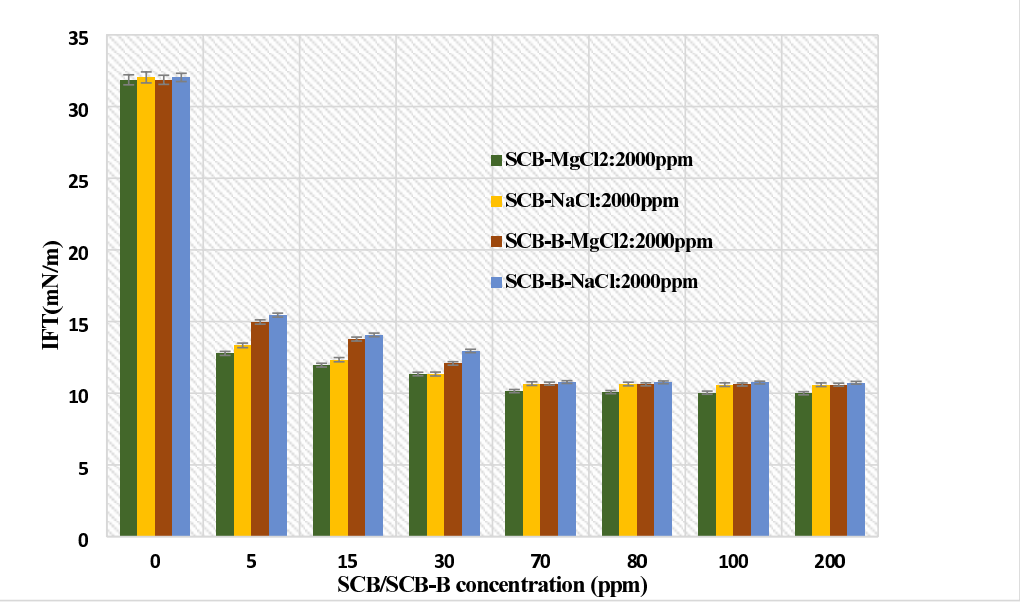

Fig. 6. Effect of different types of salinity on SCB and SCB-B induced IFT reduction at optimum salinity of 2000 ppm. Typical experimental variability ranges from ± 0.2 to 0.3 mN/m across measured IFT values.

biochar; however, as the FTIR test results showed, during the pyrolysis process, the number of hydroxyl groups in the resulting SCB-B molecules is reduced. This leads to a lower ability of Na^+ and Mg^{2+} ions to change the negative surface charge of SCB-B compared with SCB. The interaction of positively charged ions with hydroxyl ions present in bagasse biochar has been previously reported[93]. The explained electrostatic interaction can be considered one of the possible mechanisms for the interaction between the surface of SCB and SCB-B and the ions present upon the addition of salts. The ion exchange phenomenon can also be effective in this regard. As reported, the ion exchange phenomenon between the C=O double bond present in bagasse biochar and the original raw bagasse can play a crucial role in removing positive ions from an aqueous environment[94].

Finally, the reason for the reduction in final IFT difference at high concentrations of SCB and SCB-B can be attributed to the phenomenon of interaction between the aliphatic groups of adjacent molecules present on the surface of SCB and SCB-B as they come closer together at higher concentrations. This phenomenon, described in detail in the section on wettability alteration, leads to the elimination of the main factor causing the difference in hydrophobicity between SCB and SCB-B, which is the presence of aliphatic groups. Subsequently, the two materials exhibit similar behavior in reducing interfacial tension.

A schematic diagram of the governing mechanisms in interactions of SCB and SCB-B with cationic ions in the medium containing NaCl and $MgCl_2$ is presented in Fig. 7.

Investigating the effect of salinity on the SCB/SCB-B induced wettability of Oil-Wet carbonated surfaces

Finally, the effect of NaCl and $MgCl_2$ in the range of 0, 1000, and 5000 ppm at higher CMC concentrations of SCB and SCB-B was examined on the wettability alteration of oil-wet surfaces (see Figs. 8 and 9). All measurements were performed in triplicate to ensure reproducibility. As observed, both NaCl and $MgCl_2$ exhibit an inhibitory effect on the SCB and SCB-B induced wettability alteration at all concentrations. In contrast, a higher degree of wettability alteration was observed under salt-free conditions. This can be attributed to the presence of positively charged Mg^{2+} and Na^+ ions (from the dissolution of $MgCl_2$ and NaCl) and their subsequent electrostatic interactions with the negatively charged oil-wetted carbonate surface. More specifically, these ions are attracted to active sites on the negatively charged surface; as a result, the adsorption and electrostatic interaction of both SCB and SCB-B with the surface decrease. Therefore, less wettability change occurs in the presence of the examined salts. Notably, although salinity reduces the degree of wettability alteration, the results remain very promising. Both compounds change the surface's contact angle from its original value of 154° to less than 90°, which represents the optimal condition for oil recovery from a wettability perspective. It should be emphasized

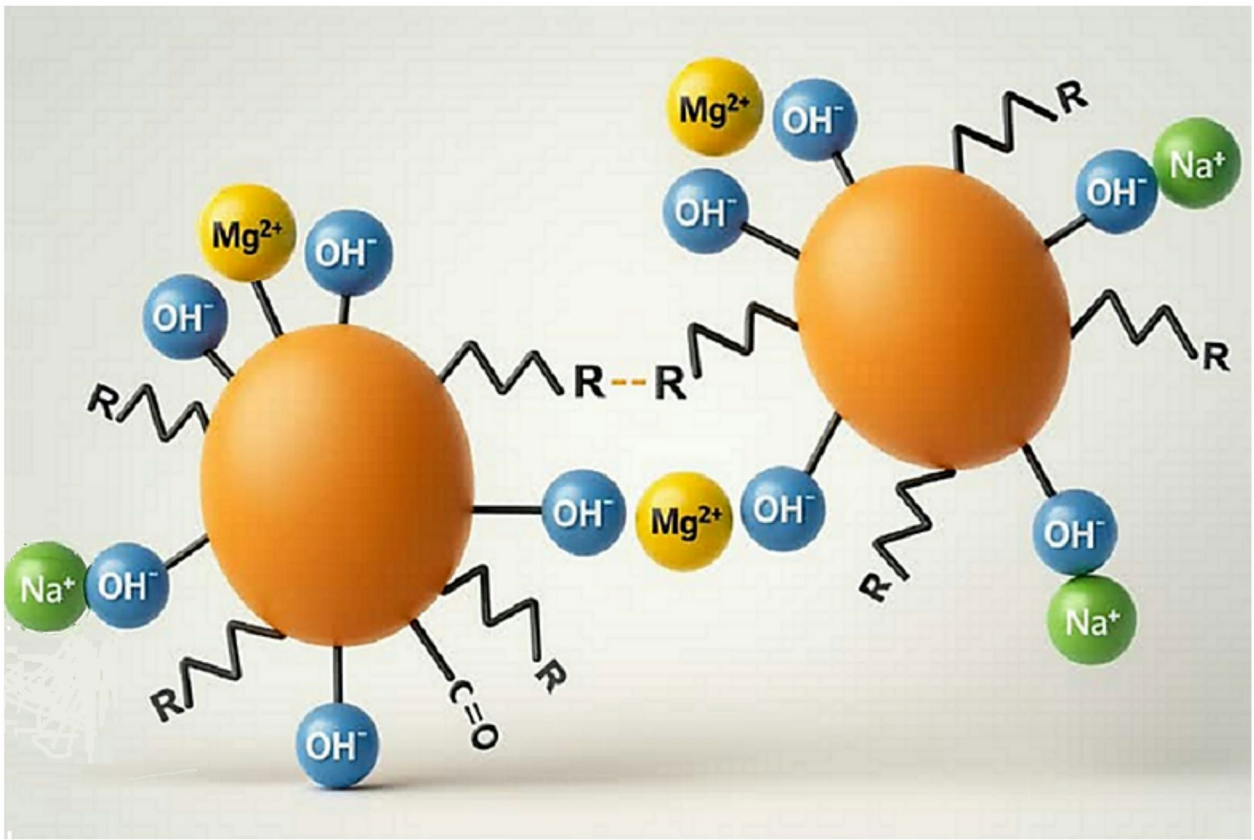

Fig. 7. Schematic diagram of probable mechanisms of SCB and SCB-B interaction in an aqueous medium containing NaCl and $MgCl_2$, including the agglomeration of aliphatic groups at high concentrations.

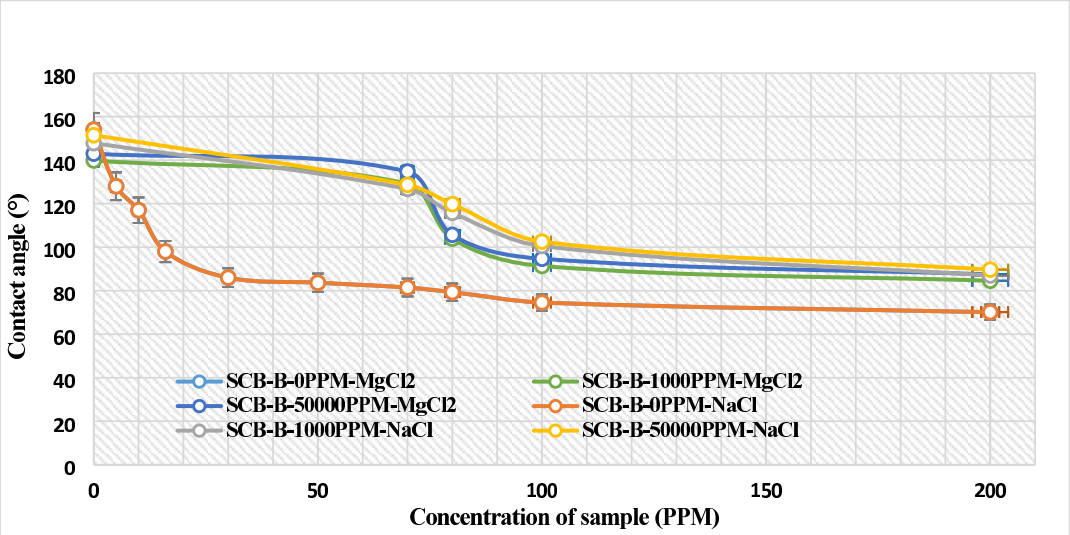

Fig. 8. Effect of NaCl and $MgCl_2$ at different concentrations on wettability alteration by SCB-B. Error bars represent the typical experimental variability, which ranges from ± 1° to 3° across the measured contact angle values.

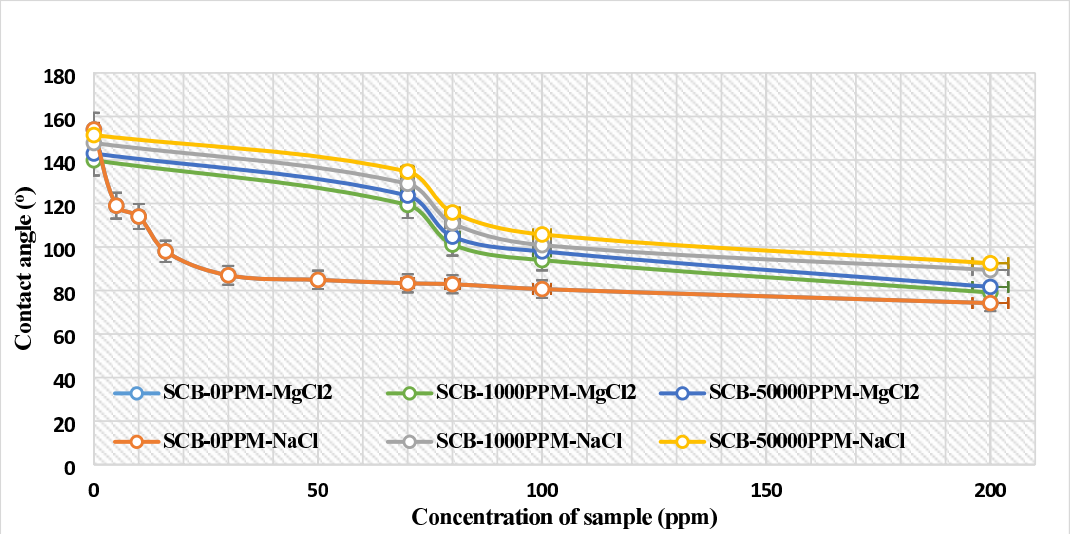

Fig. 9. Effect of NaCl and $MgCl_2$ at different concentrations on wettability alteration by SCB. Error bars represent the typical experimental variability, which ranges from ± 1° to 3° across the measured contact angle values.

that adding only 70 ppm of a low-to-zero cost waste material, which also helps address waste disposal issues, leads to significant improvements in key oil recovery parameters. Therefore, this process, being environmentally friendly and low-to-zero cost, shows great promise for the application of these materials in oil-related industries.

Moreover, the figures show that within the CMC range (70–100 ppm of SCB and SCB-B), wettability changes are more pronounced, and beyond this range, the alteration occurs more slowly. However, a different trend in wettability alteration can be observed under salt-free conditions for both SCB and SCB-B compared to saline conditions.

Finally, to further investigate the exact effect of the two salts on SCB and SCB-B induced wettability alteration, the ultimate changes in contact angle from the initial value at 200 ppm are shown in Fig. 10. Notably, greater changes in contact angle in this figure indicate a higher ability to alter wettability.

This graph shows that the salinity level did not significantly affect the final wettability alteration, as the results obtained for the low salinity condition (1000 ppm) are not substantially different from those for the high salinity condition (50,000 ppm). However, in the absence of salinity, completely different results are obtained compared to these two saline conditions. Additionally, bagasse biochar (SCB-B) induces the greatest change in

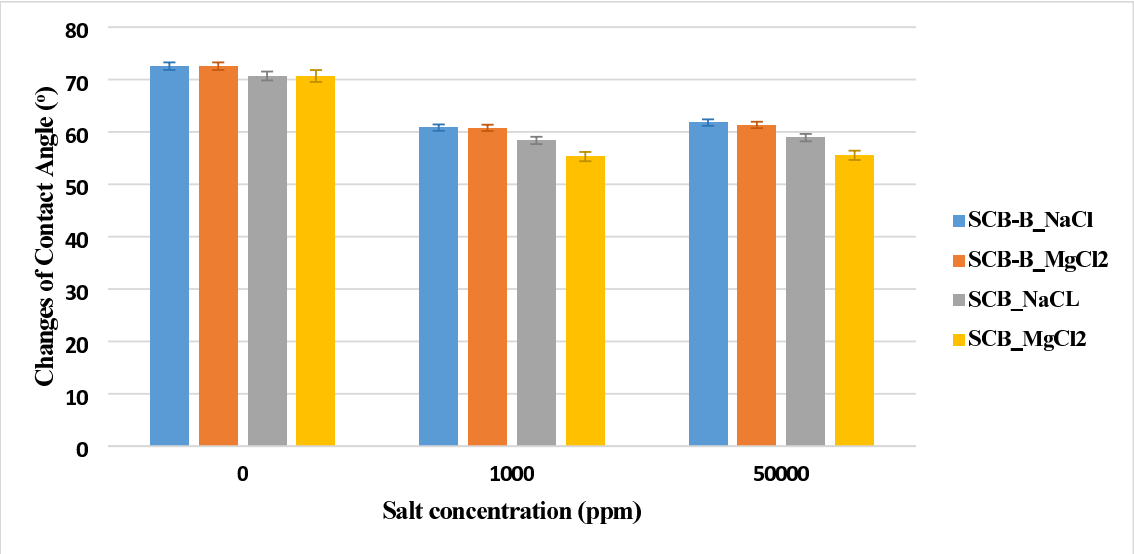

Fig. 10. Effect of NaCl and $MgCl_2$ on SCB and SCB-B induced wettability alteration at 200 ppm of compound. Error bars represent the typical experimental variability, which ranges from ± 1° to 3° across the measured contact angle values.

the wettability of oil-wetted surfaces in the presence of both types of salinity. Since this graph is based on 200 ppm of SCB and SCB-B, the results are consistent with the prevailing mechanism of wettability change under salt-free conditions at high concentrations. In other words, as observed, at concentrations higher than CMC, the interaction of aliphatic groups on the surfaces of adjacent bagasse biochar molecules, and their eventual agglomeration and potential separation from the surface, reduces the hydrophobicity of this material. Therefore, SCB-B has a greater ability to alter the wettability of oil-wet surfaces at 200 ppm.

Subsequently, raw bagasse in the presence of NaCl shows better wettability alteration than in the presence of $MgCl_2$, albeit with a small difference. This can be attributed to the greater ability of divalent Mg^{2+} ions compared to Na^{+} to inhibit the wettability alteration caused by the materials under study, as described earlier.

In total, it can be concluded that the highest degree of wettability alteration was about 47% in the presence of SCB-B under salt-free conditions and 44% in the presence of SCB-B with NaCl/$MgCl_2$ under saline conditions. These values are significant compared to other reported wettability changes caused by plant-derived natural surfactants and even many chemical surfactants or biosurfactants. For example, in 2020, Nowrouzi et al. observed a wettability change of approximately 20% when using *Anabasis Setifera* as a natural surfactant on carbonate surfaces under optimal salinity conditions of 2000 ppm from formation water[94]. Additionally, a wettability change of approximately 17.6% was observed on carbonate surfaces in the presence of oil and 15,000 ppm NaCl salinity using a cedar natural surfactant by Sofla and colleagues in 2016[81].

Implications for sustainability and circular economy

Beyond the interfacial mechanisms investigated, this work proposes a sustainable pathway aligned with circular economy principles. The primary feedstock, sugarcane bagasse, is a major agricultural residue whose conventional disposal (e.g., open burning or landfilling) contributes to environmental pollution and greenhouse gas emissions[3,7]. By repurposing it directly or via a simple pyrolysis process into a functional EOR agent, we demonstrate a waste-to-resource strategy that simultaneously addresses waste management challenges and reduces reliance on synthetic chemicals. Although a comprehensive life-cycle assessment (LCA) is beyond the scope of this foundational study, the inherent advantages are evident: the raw material is abundant, low-cost, and renewable, and its application circumvents the energy- and solvent-intensive extraction processes required for many purified plant-based surfactants[56,81]. Thus, while the direct long-term environmental footprint in reservoir conditions warrants further investigation, the use of SCB and SCB-B presents a conceptually greener and economically attractive alternative rooted in biomass valorization for the oilfield industry.

Conclusion

This study investigated the novel application of raw sugarcane bagasse (SCB) and its pyrolyzed biochar (SCB-B) as sustainable, low-cost surfactants for enhanced oil recovery (EOR). The research demonstrates that these agricultural waste materials can effectively modify key interfacial parameters—interfacial tension (IFT) and carbonate rock wettability—under both freshwater and saline conditions.

A critical finding was the identification of a distinct Critical Micelle Concentration (CMC), which served as a pivotal point for a mechanistic reversal in the behavior of both materials. The CMC was determined to be 16 ppm in the absence of salinity, increasing to 70 ppm in saline environments. Around this concentration, a notable inversion in wettability alteration efficacy was observed: SCB-B became more effective on oil-wet surfaces, while SCB performed better on water-wet surfaces at concentrations above the CMC.

Direct evidence from DLS and zeta potential analyses provided fundamental insights into this phenomenon. For SCB, a concurrent decrease in hydrodynamic diameter and increase in surface charge negativity above the CMC supports a molecular uncoiling and rearrangement mechanism, exposing more hydrophilic groups. In contrast, for SCB-B, a significant increase in particle size alongside a slight decrease in zeta potential confirms a colloidal agglomeration mechanism. This agglomeration is driven by hydrophobic interactions between the residual aliphatic groups on the rigid biochar surface, ultimately reducing its effective hydrophobicity and altering its interfacial affinity.

The introduction of salinity (NaCl and $MgCl_2$) introduced a complex influence. While an optimal salinity of 2000 ppm minimized IFT, salinity generally raised the CMC and exhibited a mild inhibitory effect on wettability alteration by occupying active sites on the rock surface. Divalent Mg^{2+} ions were more effective than monovalent Na^+ in enhancing IFT reduction, likely due to stronger interactions with the negatively charged functional groups on the biomass.

In summary, this work successfully establishes a direct link between the macroscopic performance of SCB/SCB-B in EOR-related processes and their nanoscale colloidal behavior. The discovery of the CMC-dependent mechanistic switch, validated by particle-level characterization, moves beyond mere performance reporting and offers a predictive framework for utilizing heterogeneous biomass-derived materials. The results highlight the dual promise of valorizing agricultural waste and providing an environmentally benign alternative to synthetic chemical surfactants in petroleum production. As this foundational study was conducted under ambient conditions, future work should focus on evaluating the long-term stability and oil displacement efficiency of these materials through core-flooding experiments under simulated reservoir conditions (e.g., elevated temperature and pressure).

Data availability

All data generated and analyzed during this study are included in this published article.

Received: 24 August 2025; Accepted: 29 December 2025
Published online: 06 January 2026

References

1. Kaahwa, R. M., Oyet, S. M., Muggaga, C. & Okello-Uma, I. The influence of sugarcane growing by smallholder farmers on household livelihood, food security, and nutrition status of children below five years in mid-western Uganda. *J. Agric. Food Res.* **14**, 100895 (2023).
2. Matsueda, Y. & Antunes, E. A review of current technologies for the sustainable valorisation of sugarcane Bagasse. *J. Environ. Chem. Eng.* **12**, 114900 (2024).
3. Hiranobe, C. T. et al. Sugarcane bagasse: challenges and opportunities for waste recycling. *Clean. Technol.* **6**, 662–699 (2024).
4. Trivedi, Y., Sharma, M., Mishra, R. K. & Vuppaladadiyam, A. K. Biochar potential for pollutant removal during wastewater treatment: A comprehensive review of separation mechanisms, technological integration, and process analysis. *Desalination* **600**, 118509 (2025).
5. Seah, C. C. et al. Co-pyrolysis of biomass and plastic: circularity of wastes and comprehensive review of synergistic mechanism. *Results Eng.* **17**, 100989 (2023).
6. Santos, J. V., Fregolente, L. G., Laranja, M. J. & Bisinoti, M. Hydrothermal carbonization of sugarcane industry by-products and process water reuse: Structural, morphological, and fuel properties of hydrochars. *Biomass Convers. Biorefin.* **12**, (2022).
7. Niedzwiecki, L., Moscicki, K., Bijl, A. & Pozarlik, A. Influence of hydrothermal carbonization on catalytic fast pyrolysis of agricultural biomass. *Appl. Sci.* **13**, 4190 (2023).
8. Yang, J., Zhang, Z., Wang, J. & Zhao, X. Pyrolysis and hydrothermal carbonization of biowaste: A comparative review on the conversion pathways and potential applications of Char product. *Sustain. Chem. Pharm.* **33**, 101106 (2023).
9. Tomczyk, A., Sokołowska, Z. & Boguta, P. Biochar physicochemical properties: pyrolysis temperature and feedstock kind effects. *Rev. Environ. Sci. Biotechnol.* **19**, 191–215 (2020).
10. Ethaib, S. et al. Microwave-assisted pyrolysis of biomass waste: A mini review. *Processes* **8**, 1190 (2020).
11. Jerzak, W., Acha, E. & Li, B. Comprehensive review of biomass pyrolysis: conventional and advanced technologies, reactor designs, product compositions and yields, and techno-economic analysis. *Energies* **17**, 5082 (2024).
12. Zafeer, M. K. et al. Sugarcane bagasse-based Biochar and its potential applications: a review. *Emergent Mater.* **7**, 133–161 (2023).
13. Nguyen, T. B. et al. Biochar for soil remediation: A comprehensive review of current research on pollutant removal. *Environ. Pollut.* **337**, 122571 (2023).
14. Lehmann, J. & Joseph, S. *Biochar for Environmental Management: Science, Technology and Implementation* (Routledge, 2015).
15. Woolf, D. et al. Sustainable Biochar to mitigate global climate change. *Nat. Commun.* **1**, 56 (2010).
16. Cha, J. S. et al. Production and utilization of biochar: A review. *J. Ind. Eng. Chem.* **40**, 1–15 (2016).
17. Akca, M. O. et al. Engineering the Biochar surfaces through feedstock variations and pyrolysis temperatures. *Ind. Crops Prod.* **218**, 118819 (2024).
18. Brown, T. R., Wright, M. & Brown, R. C. Estimating profitability of two Biochar production scenarios: slow pyrolysis vs fast pyrolysis. *Biofuels Bioprod. Biorefining.* **5**, 54–68 (2011).
19. Lonappan, L., Liu, Y., Rouissi, T. & Brar, S. K. Development of biochar-based green functional materials using organic acids for environmental applications. *J. Clean. Prod.* **244**, 118841 (2019).
20. Sharma, P. Biochar application for sustainable soil erosion control: a review of current research and future perspectives. *Front. Environ. Sci.* **12**, 1373287 (2024).
21. Machado, A. R. T., Carolino, J. M., Braz, G. S. & Machado, A.R.T. Assessment of the ecotoxicity of extracts from sugarcane Bagasse biochars activated with zinc chloride. *Environ. Chem. Ecotoxicol.* **7**, 19–26 (2025).
22. Liu, Y. et al. Recent studies on the comprehensive application of Biochar in multiple environmental fields. *J. Clean. Prod.* **421**, 138495 (2023).
23. Khan, S. et al. Biochar production and characteristics, its impacts on soil health, crop production, and yield enhancement: A review. *Plants* **13**, 166 (2024).
24. Haider, M. I. S. et al. Synergistic interactions and reaction mechanisms of Biochar surface functionalities in antibiotics removal from industrial wastewater. *Environ. Pollut.* **356**, 124365 (2024).
25. Chen, J. et al. The estimation of the higher heating value of Biochar by data-driven modeling. *J. Renew. Mater.* **10**, 1555–1574 (2022).
26. Saletnik, B. Opportunities and threats for supercapacitor technology based on biochar: A review. *Energies* **17**, 4617 (2024).

27. Firozjaii, A. M. & Saghafi, H. R. Review on chemical enhanced oil recovery using polymer flooding: Fundamentals, experimental and numerical simulation. *Petroleum* **6**, 115–122 (2020).
28. Sarafzadeh, P. et al. Enterobacter cloacae as biosurfactant producing bacterium: differentiating its effects on interfacial tension and wettability alteration Mechanisms for oil recovery during MEOR process. *Colloids Surf. B Biointerfaces*. **105**, 223–229 (2013).
29. Sarafzadeh, P. et al. Investigating the efficiency of MEOR processes using enterobacter cloacae and bacillus stearothermophilus SUCPM#14 (biosurfactant-producing strains) in carbonated reservoirs. *J. Pet. Sci. Eng.* **113**, 46–53 (2013).
30. Sarafzadeh, P. et al. Modification of rock/fluid and fluid/fluid interfaces during MEOR processes, using two biosurfactant producing strains of *Bacillus stearothermophilus* SUCPM#14 and *Enterobacter cloacae*: A mechanistic study. *Colloids Surf. B Biointerfaces*. **117**, 457–465 (2014).
31. Ghorbani, M. et al. Modification and mechanistic study of fluid/fluid and carbonate rock/fluid interfaces using a glycolipid biosurfactant from an indigenous strain of Gordonia terrae for MEOR applications. *J. Mol. Liq.* **414**, 126198 (2024).
32. Alkan, H., Mukherjee, S. & Jelinek, W. Front-end engineering practice of in-situ MEOR applications. *J. Pet. Sci. Eng.* **216**, 110407 (2022).
33. Fernandes, P. L. et al. Microbial enhanced oil recovery: use of metabolic products of Bacillus subtilis RI4914 in non-consolidated porous media and influence of environmental parameters. *Colloids Surf. Physicochem. Eng. Asp*. **697**, 134431 (2024).
34. Chen, Z. et al. Insights into wettability alteration mechanisms of microbial enhanced oil recovery by different biosurfactants in sandstone oil reservoir. *Colloids Surf. Physicochem. Eng. Asp*. **691**, 133889 (2024).
35. Abdi, A. et al. Effect of bacteria on oil/water interfacial tension in asphaltenic oil reservoirs. *Colloids Surf. Physicochem. Eng. Asp*. **639**, 128263 (2022).
36. Xia, W. J., Dong, H. P., Yu, L. & Yu, D. F. Comparative study of biosurfactant produced by microorganisms isolated from formation water of petroleum reservoir. *Colloids Surf. Physicochem. Eng. Asp*. **392**, 124–130 (2011).
37. Salam, A. H. et al. A perspective on ionic liquids as multifunctional agents in enhanced oil recovery and CO2 sequestration in carbonate formations. *Carbon Capture Sci. Technol.* **15**, 100443 (2025).
38. Yu, H. et al. Experimental investigation on conformance control and EOR-CO2 sequestration of non-chemical CO2 microbubbles in low permeability reservoirs. *Geoenergy Sci. Eng.* **254**, 214019 (2025).
39. Uoda, M. K., Hussein, H. Q. & Jalil, R. R. Experimental investigation of combined carbon nanoparticles (CNPs), ionic liquid (I.L), and low salinity water to enhance oil recovery (EOR) at iraq's Southern oil fields. *J. Mol. Liq*. **391**, 123322 (2023).
40. Tafur, N. et al. Assessment of a surface-active ionic liquid formulation for EOR applications: experimental and simulation studies. *Geoenergy Sci. Eng.* **224**, 211619 (2023).
41. Somoza, A., Tafur, N., Arce, A. & Soto, A. Design and performance analysis of a formulation based on SDBS and ionic liquid for EOR in carbonate reservoirs. *J. Pet. Sci. Eng.* **209**, 109856 (2022).
42. Ding, K. et al. An ionic liquid-present hydrothermal method for Preparing Hawthorn Sherry ball shaped palladium (Pd)-based composite catalysts for ethanol oxidation reaction (EOR). *Int. J. Hydrogen Energy*. **45**, 1930–1939 (2020).
43. Wang, X. et al. A composite system of amphoteric copolymer nanosphere and betaine surfactant for enhanced oil recovery application. *Colloids Surf. Physicochem. Eng. Asp*. **718**, 136933 (2025).
44. Fang, Z., Cao, X. R., Yu, Y. L. & Li, M. Fabrication and characterization of microcapsule encapsulating EOR surfactants by microfluidic technique. *Colloids Surf. Physicochem. Eng. Asp*. **570**, 282–292 (2019).
45. Gazem, A. et al. Combined effect of silica nanoparticles and binary surfactants in enhancing oil recovery: an experimental investigation. *Colloids Surf. Physicochem. Eng. Asp*. **702**, 134980 (2024).
46. Nafisifar, A., Manshad, A. K. & Shadizadeh, S. R. Evaluation of a new green synthesized surfactant from linseeds—chemical EOR implications from sandstone petroleum reservoirs. *J. Mol. Liq*. **342**, 117263 (2021).
47. Behdadfar, M. H., Sheng, J. J. & Esmaeilnezhad, E. Designing effective enhanced oil recovery fluid: combination of graphene oxide, D118 SuperPusher, and Chuback surfactant. *J. Mol. Liq*. **390**, 123081 (2023).
48. Samiei Nezhad, M., Wood, D. A., Sadatshojaei, E. & Esmaeilzadeh, F. New insight to experimental study of ionic solutions with a non-ionic surfactant on wettability, interfacial tension and micro-model flooding. *Fuel* **285**, 119126 (2021).
49. Zaeri, M. R. et al. Study of the effect of acid number on the interfacial tension between carbon dioxide and different combinations of diesel fuel and gasoline at different pressures. *Arab. J. Sci. Eng.* **49**, 8543–8554 (2024).
50. Ghanaatian, A. et al. Coating SiO2 nanoparticles with Polyvinyl alcohol for interfacial tension alteration in the system CO2 + polyethylen glycol + water. *Surf. Interfaces*. **32**, 102164 (2022).
51. Elhambakhsh, A. et al. Experimental evaluation of acid number effect on interfacial tension between nitrogen and mixtures of petroleum fractions including diesel fuel and gasoline at different pressures. *Sci. Rep.* **14**, 24806 (2024).
52. Schexnayder, P., Baudoin, N. & Chirdon, W. M. Enhanced oil recovery from denatured algal biomass: synergy between conventional and emergent fuels. *Fuel* **287**, 119533 (2021).
53. Bachari, Z. Application of natural surfactants for enhanced oil recovery –Critical review. *IOP Conf. Ser. Earth Environ. Sci.* **221**, 012039 (2019).
54. Zhan, Y. et al. Potential of wheat Bran to promote Indigenous microbial enhanced oil recovery. *J. Ind. Microbiol. Biotechnol.* **44**, 845–855 (2017).
55. Chhetri, A. B., Watts, K. C., Rahman, M. S. & Islam, M. R. Soapnut extract as a natural surfactant for enhanced oil recovery. *Energy Sources Part. A*. **31**, 1893–1903 (2009).
56. Ahmadi, M. A., Zendehboudi, S., Shafiei, A. & James, L. Nonionic surfactant for enhanced oil recovery from carbonates: adsorption kinetics and equilibrium. *Ind. Eng. Chem. Res.* **51**, 9894–9905 (2012).
57. Deymeh, H., Shadizadeh, S. R. & Motafakkerfard, R. Experimental investigation of Seidlitzia Rosmarinus effect on oil-water interfacial tension: usable for chemical enhanced oil recovery. *Sci. Iran.* **19**, 1661–1664 (2012).
58. Pordel Shahri, M., Shadizadeh, S. R. & Jamialahmadi, M. Applicability test of new surfactant produced from Zizyphus Spina-Christi leaves for enhanced oil recovery in carbonate reservoirs. *J. Japan Pet. Inst.* **55**, 27–32 (2012).
59. Azdarpour, A., Mohammadian, E., Norouzpour, N. & Liu, B. The effects of a novel Bio-based surfactant derived from the acacia concinna plant on chemical enhanced oil recovery in the presence of various salts and a synthesized HSPAM polymer. *J Mol. Liq* **386**, (2023).
60. Jafari Pour, M., Khaksar Manshad, A., Zargar, G. & Akbari, M. Application of a new anionic surfactant based on Sesame oil by Alkali-Surfactant (AS) injection in chemical enhanced oil recovery: Characterization, mechanisms and performance. *J Mol. Liq* **395**, (2024).
61. Mousavi Dashtaki, S. R. et al. Evaluation the role of natural surfactants from tanacetum and Tarragon plants in EOR applications. *J. Mol. Liq.* **361**, (2022).
62. Navaie, F., Esmaeilnezhad, E. & Choi, H. J. Xanthan gum-added natural surfactant solution of chuback: A green and clean technique for enhanced oil recovery. *J. Mol. Liq.* **354**, (2022).
63. Azdarpour, A., Mohammadian, E., Norouzpour, M. & Liu, B. The effects of a novel Bio-based surfactant derived from the acacia concinna plant on chemical enhanced oil recovery in the presence of various salts and a synthesized HSPAM polymer. *J. Mol. Liq.* **386**, (2023).
64. Razzaghi-Koolaee, F. et al. A comprehensive study on the application of a natural plant-based surfactant as a chemical enhanced oil recovery (CEOR) agent in the presence of different ions in carbonate reservoirs. *J. Environ. Chem. Eng.* **10**, (2022).
65. Nandwani, S. K. et al. Study on interfacial properties of imidazolium ionic liquids as surfactant and their application in enhanced oil recovery. *Colloids Surf. Physicochem. Eng. Asp*. **516**, 383–393 (2017).

66. Jia, H. et al. Systematic investigation of the effects of mixed cationic/anionic surfactants on the interfacial tension of a water/model oil system and their application to enhance crude oil recovery. *Colloids Surf. Physicochem. Eng. Asp*. **529**, 621–627 (2017).
67. Bak, A. & Podgorska, W. Interfacial and surface tensions of toluene/water and air/ water systems with nonionic surfactants tween 20 and tween 80. *Colloids Surf. Physicochem. Eng. Asp*. **504**, 414–425 (2016).
68. Jia, H. et al. Systematic investigation of the synergistic effects of novel biosurfactant ethoxylated phytosterol-alcohol systems on the interfacial tension of a water/model oil system. *Colloids Surf. Physicochem. Eng. Asp*. **513**, 292–296 (2017).
69. Ye, Z. et al. The effect of temperature on the interfacial tension between crude oil and gemini surfactant solution. *Colloids Surf. Physicochem. Eng. Asp*. **322**, 138–141 (2008).
70. Liu, S. Y. et al. Wettability modification and restraint of moisture re-adsorption of lignite using cationic gemini surfactant. *Colloids Surf. Physicochem. Eng. Asp*. **508**, 286–293 (2016).
71. Schimmelpfennig, S. & Glaser, B. One step forward toward characterization: some important material properties to distinguish biochars. *J. Environ. Qual.* **41**, 1001–1013 (2012).
72. Chen, X. et al. Adsorption of copper and zinc by biochars produced from pyrolysis of hardwood and corn straw in aqueous solution. *Bioresour Technol.* **102**, 8877–8884 (2011).
73. Hammes, K. et al. Synthesis and characterisation of laboratory-charred grass straw (Oryza sativa) and chestnut wood (Castanea sativa) as reference materials for black carbon quantification. *Org. Geochem*. **37**, 1629–1633 (2006).
74. Londoño-Restrepo, S. M. et al. In-situ XRD study of the crystal size transition of hydroxyapatite from swine bone. *Ceram. Int.* **46**, 24454–24461 (2020).
75. Mehrabianfar, P., Malmir, P., Soulgani, B. S. & Hashemi, A. Study on the optimization of the performance of preformed particle gel (PPG) on the isolation of high permeable zone. *J. Pet. Sci. Eng.* **195**, 107530 (2020).
76. Zhao, T. & Jiang, L. Contact angle measurement of natural materials. *Colloids Surf. B Biointerfaces*. **161**, 324–330 (2018).
77. Zhang, X. et al. Determining the surface tension of two-dimensional nanosheets by a low-rate advancing contact angle measurement. *Langmuir* **35**, 8308–8315 (2019).
78. Qiao, W., Li, J., Zhu, Y. & Cai, H. Interfacial tension behavior of double long-chain 1, 3, 5-triazine surfactants for enhanced oil recovery. *Fuel* **96**, 220–225 (2012).
79. Lim, S. et al. A review on the mechanisms of low salinity water/surfactant/nanoparticles and the potential synergistic application for c-EOR. *Pet. Res.* **8**, 324–337 (2023).
80. Jafari Daghlian Sofla, S., Sharifi, M. & Hemmati Sarapardeh, A. Toward mechanistic Understanding of natural surfactant flooding in enhanced oil recovery processes: the role of salinity, surfactant concentration and rock type. *J. Mol. Liq*. **222**, 632–639 (2016).
81. Haq, B. Green enhanced oil recovery for carbonate reservoirs. *Polymers* **13**, 3269 (2021).
82. Haq, B. et al. Date-Leaf carbon particles for green enhanced oil recovery. *Nanomaterials* **12**, 1245 (2020).
83. Ghaffari, A. et al. Examining the effect of reservoir conditions on efficiency of microbial enhanced oil recovery processes using Rhodococcus erythropolis strain; experimental approach. *Braz J. Chem. Eng.* **40**, 573–583 (2022).
84. Kinney, T. J. et al. Hydrologic properties of biochars produced at different temperatures. *Biomass Bioenergy*. **41**, 34–43 (2012).
85. Gray, M., Johnson, M. G., Dragila, M. I. & Kleber, M. Water uptake in biochars: the roles of porosity and hydrophobicity. *Biomass Bioenergy*. **61**, 196–205 (2014).
86. Das, O. & Sarmah, A. K. The love-hate relationship of pyrolysis Biochar and water: A perspective. *Sci. Total Environ.* **512**, 682–685 (2015).
87. Mecinovic, J. et al. Fluoroalkyl and alkyl chains have similar hydrophobicities in binding to the hydrophobic wall of carbonic anhydrase. *J. Am. Chem. Soc.* **133**, 14017–14026 (2011).
88. Nyah, F. et al. Comprehensive review on the role of salinity on oil recovery mechanisms during chemical flooding. *J. Mol. Liq* **415**, (2024).
89. Hoffmann, M. M., Darab, J. G., Fulton, J. L. & Pfund, D. M. A fluorescence spectroscopic and molecular dynamics study of the aggregation of lignin in NaOH/Water solvents. *J. Phys. Chem. A*. **105**, 1772–1782 (2001).
90. Al-Rudaini, G. S. N. A. & Khalil, K. M. S. Colloidal properties of lignosulfonate in aqueous solutions: the effect of pH and concentration. *J. Dispersion Sci. Technol.* **39**, 128–136 (2018).
91. Norgren, M. & Edlund, H. Lignin: Recent advances and emerging applications. *Curr. Opin. Colloid Interface Sci.* **19**, 409–416 (2014).
92. de Eugênio, A. et al. Biochars from modified sugarcane Bagasse for manganese removal from mining effluents. *J. Environ. Chem. Eng.* **11**, 110761 (2023).
93. Manyatshe, A. et al. Chitosan modified sugarcane Bagasse Biochar for the adsorption of inorganic phosphate ions from aqueous solution. *J. Environ. Chem. Eng.* **10**, 108243 (2022).
94. Nowrouzi, I., Mohammadi, A. H. & Manshad, A. K. Water-oil interfacial tension (IFT) reduction and wettability alteration in surfactant flooding process using extracted saponin from anabasis setifera plant. *J. Pet. Sci. Eng.* **189**, 106901 (2020).

Acknowledgements

The authors are grateful to the Shiraz University for supporting this research.

Author contributions

P.S.: Conceptualization, methodology, investigation, writing—original draft. F.E.: Conceptualization, methodology, supervision, writing—review and editing. K.M.: Investigation, formal analysis. S.S.: Conceptualization, writing—review and editing. G.V.-N.: Validation, resources, writing—review and editing. All authors reviewed the manuscript.

Funding

There is no funding to declare.

Declarations

Competing interests

The authors declare no competing interests.

Additional information

Supplementary Information The online version contains supplementary material available at https://doi.org/10.1038/s41598-025-34517-y.

Correspondence and requests for materials should be addressed to F.E. or S.S.